

Inferring interactions of time-delayed dynamic networks by random state variable resetting

Changbao Deng(邓长宝), Weinuo Jiang(蒋未诺), and Shihong Wang(王世红)
Citation: Chin. Phys. B, 2022, 31 (**3**): 030502. DOI: 10.1088/1674-1056/ac1e12
Journal homepage: http://cpb.iphy.ac.cn; http://iopscience.iop.org/cpb

What follows is a list of articles you may be interested in

Stabilization strategy of a car-following model with multiple time delays of the drivers

Weilin Ren(任卫林), Rongjun Cheng(程荣军), and Hongxia Ge(葛红霞)
Chin. Phys. B, 2021, 30 (**12**): 120506. DOI: 10.1088/1674-1056/abfcc9

Physical generation of random numbers using an asymmetrical Boolean network

Hai-Fang Liu(刘海芳), Yun-Cai Wang(王云才), Lu-Xiao Sang(桑鲁骁), and Jian-Guo Zhang(张建国)
Chin. Phys. B, 2021, 30 (**11**): 110503. DOI: 10.1088/1674-1056/abf4fc

Stochastic bounded consensus of second-order multi-agent systems in noisy environment

Hong-Wei Ren(任红卫), Fei-Qi Deng(邓飞其)
Chin. Phys. B, 2017, 26 (**10**): 100506. DOI: 10.1088/1674-1056/26/10/100506

Effects of time delays in a mathematical bone model

Li-Fang Wang(王莉芳), Kang Qiu(仇康), Ya Jia(贾亚)
Chin. Phys. B, 2017, 26 (**3**): 030503. DOI: 10.1088/1674-1056/26/3/030503

Cluster synchronization of community network with distributed time delays via impulsive control

Hui Leng(冷卉), Zhao-Yan Wu(吴召艳)
Chin. Phys. B, 2016, 25 (**11**): 110501. DOI: 10.1088/1674-1056/25/11/110501

Inferring interactions of time-delayed dynamic networks by random state variable resetting

Changbao Deng(邓长宝), Weinuo Jiang(蒋未诺), and Shihong Wang(王世红)†

School of Sciences, Beijing University of Posts and Telecommunications, Beijing 100876, *China*

(Received 19 April 2021; revised manuscript received 20 July 2021; accepted manuscript online 17 August 2021)

Time delays exist widely in real systems, and time-delayed interactions can result in abundant dynamic behaviors and functions in dynamic networks. Inferring the time delays and interactions is challenging due to systematic nonlinearity, noises, a lack of information, and so on. Recently, Shi *et al.* proposed a random state variable resetting method to detect the interactions in a continuous-time dynamic network. By arbitrarily resetting the state variable of a driving node, the equivalent coupling functions of the driving node to any response node in the network can be reconstructed. In this paper, we introduce this method in time-delayed dynamic networks. To infer actual time delays, the nearest neighbor correlation (NNC) function for a given time delay is defined. The significant increments of NNC originate from the delayed effect. Based on the increments, the time delays can be reconstructed and the reconstruction errors depend on the sampling time interval. After time delays are accurately identified, the equivalent coupling functions can also be reconstructed. The numerical results have fully verified the validity of the theoretical analysis.

Keywords: time delays, network reconstruction, random state variable resetting

PACS: 05.45.–a, 64.60.aq, 89.75.Fb **DOI:** 10.1088/1674-1056/ac1e12

1. Introduction

Complex dynamic networks are used to model interacting individuals in interdisciplinary research.[1–6] Due to the limited propagation speed of signals, time delays play a significant role and exist extensively in real systems.[7–11] Detecting the interactions in networks is helpful for understanding the collective behaviors of complex systems. However, due to systematic nonlinearity, noises, a lack of information, time delays, and so on, inferring the interactions in dynamic networks is complicated and challenging. Some methods have been proposed for inferring the interactions without time delays. Typical statistical methods, such as cross correlation,[12] Granger causality,[13] mutual information,[14] and transfer entropy,[15] are usually used to define functional connections, which provide limited information for interacting nodes. In recent years, researchers have explored approaches to inferring the interactions by solving ordinary differential equations (ODEs). Some detection methods can be used to reconstruct a linear dynamic network,[16–19] while expanding basis[20–24] and expanding variable[25,26] methods are proposed to detect a general nonlinear dynamic network. These methods not only reveal connections, but also provide information on local dynamics and coupling functions. For these methods,[20–26] solving ODEs requires the output data of the whole network. The existence of noises increases the difficulty of network reconstruction, sometimes, also leading to new approaches.[27,28] In Refs. [27,28], the injection of noise into the nodes enhances the target interaction and weakens the effect of hidden nodes and variables. In addition, there are some proactive methods, such as driving-response controlling,[3] copy-synchronization,[3] and random phase resetting.[29]

For time-delayed dynamic networks, accurately identifying delays is the prerequisite for network reconstruction. There are several existing methods for identification of time delays, such as parameter estimation,[30] adaptive synchronization,[31,32] model-fitting approaches,[30,31] perturbation methods,[32,33] the permutation-information-theory approach,[34] and cross map evaluation.[35] However, most of these methods are appropriate in a single dynamic system. In a dynamic network, a large number of time-delayed interactions make network reconstruction extremely difficult. Recently, Zhang *et al.* proposed a new method to detect time delays and the average coupling strengths through the correlations induced by fast-varying noises (here called FVN).[36]

The random state variable resetting (RSVR)[37,38] method proposed by Shi *et al.*, as an active control method, can be used to detect the interactions in dynamical networks. By randomly resetting the state variable of a driving node, the influence of other nodes and variables on a response node can be simplified as background average and fluctuations, and then the equivalent coupling function of a driving node to a response node can be reconstructed using only the data of two related nodes. In this paper, we introduce the RSVR method to reconstruct time-delayed dynamic networks. Based on the output data after randomly resetting, we define the nearest neighbor correlation (NNC) function for a given time delay. According to the increment of the defined NNC at the actual time delay, we can identify the time delay accurately. The error of determined

†Corresponding author. E-mail: shwang@bupt.edu.cn

© 2022 Chinese Physical Society and IOP Publishing Ltd

time delays only depends on the sampling time interval. Compared with the FVN method,[36] the NNC function defined through RSVR is effective even for a relatively low sampling frequency. After the time delay is determined, the equivalent directed time-delayed coupling function can be reconstructed from measurable data. By arbitrarily resetting the variable of a driving node, the RSVR method can infer the time delays and equivalent directed time-delayed coupling functions of the driving node to the other response nodes. In actual networks, some nodes and variables are not measurable. This reconstruction method is applicable to networks with hidden nodes and variables.

2. Method

We consider a time-delayed dynamic network

$$\begin{aligned}\dot{x}_i(t) &= f_i(x_i(t),\boldsymbol{v}_i(t)) \\ &\quad +\sum_{j\neq i}^{N} h_{ij}(x_i(t),x_j(t-\tau_{ij}))+\eta_i(t), \qquad (1)\\ \dot{\boldsymbol{v}}_i(t) &= \boldsymbol{g}_i(x_i(t),\boldsymbol{v}_i(t)), \qquad (2)\end{aligned}$$

where x_i and $\boldsymbol{v}_i$ denote the state variables of node i, x_i is measurable and $\boldsymbol{v}_i$ is hidden. $f_i(x_i,\boldsymbol{v}_i(t))$ and $\boldsymbol{g}_i(x_i,\boldsymbol{v}_i(t))$ denote the local dynamics of node i. $h_{ij}(x_i(t),x_j(t-\tau_{ij}))$ represents the coupling function from node j to node i, and τ_{ij} denotes time delays. $i,j=1,2,\ldots,N$, N being the size of network, i.e., the total number of nodes in the network. η_i represents white noises with

$$\langle\eta_i(t)\rangle=0,\quad \langle\eta_i(t)\eta_j(t')\rangle=Q_i\delta_{ij}\delta(t-t'), \qquad (3)$$

where $\langle\cdot\rangle$ denotes the average. Q_i represents the intensity of white noises. $\delta_{ij}=1$ if $i=j$, otherwise $\delta_{ij}=0$.

Now we introduce the random variable resetting method to detect how x_j influences x_i with the time delay τ_{ij}. We assume that we can randomly reinitialize the state variable x_j M times, $M\gg 1$. And after each initialization, we can continue to record the state of all measurable variables for a period of time, so then we get the following data:

$$\begin{array}{ccccccc} x_j(t_1) & x_i(t_1) & x_i(t_1+\Delta t) & x_i(t_1+2\Delta t) & \cdots & x_i(t_1+n_{\max}\Delta t)\\ x_j(t_2) & x_i(t_2) & x_i(t_2+\Delta t) & x_i(t_2+2\Delta t) & \cdots & x_i(t_2+n_{\max}\Delta t)\\ \vdots & \vdots & \vdots & \vdots & \ddots & \vdots\\ x_j(t_m) & x_i(t_m) & x_i(t_m+\Delta t) & x_i(t_m+2\Delta t) & \cdots & x_i(t_m+n_{\max}\Delta t)\\ \vdots & \vdots & \vdots & \vdots & \ddots & \vdots\\ x_j(t_M) & x_i(t_M) & x_i(t_M+\Delta t) & x_i(t_M+2\Delta t) & \cdots & x_i(t_M+n_{\max}\Delta t)\end{array} \qquad (4)$$

where $i=1,2,\ldots,N$, Δt denotes sampling time interval, measurement time interval $\tau_{\text{measure}}=n_{\max}\Delta t$, and resetting time interval $\tau_{\text{reset}}=t_{m+1}-t_m$, $\tau_{\text{reset}}>\tau_{\text{measure}}$. The resetting time interval τ_{reset} can be a constant or a random value; without loss of generality, we take random reset intervals in this paper. For each reinitialization and the time delay τ, the effect of other variables (or nodes) on node i can be simplified as an average of M measurements and its fluctuations,[38] and therefore Eq. (1) can be rewritten as

$$\dot{x}_i(t_m+\tau)=h'_{ij}(x_j(t_m),\tau)+b_{ij}(\tau)+r_{ij}(t_m+\tau), \qquad (5)$$

where $\dot{x}_i(t_m+\tau)=[x_i(t_m+\tau+\Delta t)-x_i(t_m+\tau)]/\Delta t$, $h'_{ij}(x_j(t_m),\tau)$ denotes the equivalent coupling function of node j to node i with the time delay τ, and $b_{ij}(\tau)$ and $r_{ij}(t_m+\tau)$ describe the statistical average of M times and its fluctuations, respectively. The fluctuations in Eq. (5) have the following statistical characteristics:

$$\langle r_{ij}(t_m+\tau)\rangle=0, \qquad (6)$$

$$\langle r_{ij}(t_m+\tau)F(x_j(t_m))\rangle=0,\quad \tau\leq\tau_{ij}, \qquad (7)$$

where $F(x_j(t_m))$ can be any given function.

Due to the time delay in Eq. (1), the equivalent coupling function $h'_{ij}(x_j(t_m),\tau)$ has the following characteristics:

$$h'_{ij}(x_j(t_m),\tau)\begin{cases}=0, & \tau<\tau_{ij},\\ \neq 0, & \tau=\tau_{ij},\end{cases} \qquad (8)$$

where $h'_{ij}(x_j(t),\tau_{ij})$ denotes the equivalent coupling function of node j to node i with the actual time delay τ_{ij}.

For nonlinear systems, the fluctuations in Eq. (5) are generally relatively large. To reduce the influence of fluctuations, we consider smoothing the data $\dot{x}_i(t_m+\tau)$, and therefore we rewrite Eq. (5) as

$$\dot{\boldsymbol{x}}_i(x_j,\tau)=h'_{ij}(x_j,\tau)+b_{ij}(\tau)+\boldsymbol{r}_{ij}(x_j,\tau), \qquad (9)$$

where $\dot{\boldsymbol{x}}_i(x_j,\tau)$ and $\boldsymbol{r}_{ij}(x_j,\tau)$ denote the smoothed results. In this paper, we introduce the Dirac kernel function to calculate $\dot{\boldsymbol{x}}_i(x_j,\tau)$ by

$$\dot{\boldsymbol{x}}_i(x_j,\tau)=\frac{\sum_{m=1}^{M}Q(x_j-x_j(t_m))\dot{x}_i(t_m+\tau)}{\sum_{m=1}^{M}Q(x_j-x_j(t_m))}, \qquad (10)$$

where the Dirac kernel function $Q(x)=\int_{x-\frac{d}{2}}^{x+\frac{d}{2}}\delta(x')\,\mathrm{d}x'$, d being the smoothing window.

Subtracting the respective mean values from both sides of Eq. (9), we then get

$$\begin{aligned}\dot{\boldsymbol{x}}_i(x_j,\tau)-\langle\dot{\boldsymbol{x}}_i(x_j,\tau)\rangle &= h'_{ij}(x_j,\tau)-\langle h'_{ij}(x_j,\tau)\rangle\\ &\quad +b_{ij}(\tau)-\langle b_{ij}(\tau)\rangle\\ &\quad +\boldsymbol{r}_{ij}(x_j,\tau)-\langle\boldsymbol{r}_{ij}(x_j,\tau)\rangle, \qquad (11)\end{aligned}$$

where $\langle\dot{\boldsymbol{x}}_i(x_j,\tau)\rangle$ denotes the average of all the smoothed $\dot{\boldsymbol{x}}_i(x_j,\tau)$, and can be calculated. Accordingly, $\langle h'_{ij}(x_j,\tau)\rangle$, $\langle b_{ij}(\tau)\rangle$, and $\langle\boldsymbol{r}_{ij}(x_j,\tau)\rangle$ also represent the averages of $h'_{ij}(x_j,\tau)$, $b_{ij}(\tau)$, and $\boldsymbol{r}_{ij}(x_j,\tau)$, respectively. Since $b_{ij}(\tau)$ is a constant and $\langle\boldsymbol{r}_{ij}(x_j,\tau)\rangle=0$, we can rewrite Eq. (11) as

$$\begin{aligned}\dot{\boldsymbol{x}}_i(x_j,\tau)-\langle\dot{\boldsymbol{x}}_i(x_j,\tau)\rangle &= h'_{ij}(x_j,\tau)-\langle h'_{ij}(x_j,\tau)\rangle\\ &\quad +\boldsymbol{r}_{ij}(x_j,\tau). \qquad (12)\end{aligned}$$

To determine the time delay of node j to node i in Eq. (1),

we first define the nearest neighbor correlation (NNC) function with the time delay τ as

$$\begin{aligned}&\mathrm{NNC}_{ij}(\tau)\\&=\left\langle\left(\dot{\boldsymbol{x}}_i(x_j,\tau)-\left\langle\dot{\boldsymbol{x}}_i(x_j,\tau)\right\rangle\right)\left(\dot{\boldsymbol{x}}_i(x_j+d,\tau)-\left\langle\dot{\boldsymbol{x}}_i(x_j,\tau)\right\rangle\right)\right\rangle.\end{aligned}\tag{13}$$

Then we calculate the nearest neighbor correlations of both sides of Eq. (12), and we have

$$\begin{aligned}&\left\langle\left(\dot{\boldsymbol{x}}_i(x_j,\tau)-\left\langle\dot{\boldsymbol{x}}_i(x_j,\tau)\right\rangle\right)\left(\dot{\boldsymbol{x}}_i(x_j+d,\tau)-\left\langle\dot{\boldsymbol{x}}_i(x_j,\tau)\right\rangle\right)\right\rangle\\&=\left\langle\left(h'_{ij}(x_j,\tau)-\langle h'_{ij}(x_j,\tau)\rangle+\boldsymbol{r}_{ij}(x_j,\tau)\right)\left(h'_{ij}(x_j+d,\tau)\right.\right.\\&\quad\left.\left.-\left\langle h'_{ij}(x_j,\tau)\right\rangle+\boldsymbol{r}_{ij}(x_j+d,\tau)\right)\right\rangle.\end{aligned}\tag{14}$$

Due to random state variable resetting, variable-fluctuation correlation and fluctuation-fluctuation correlation approximately vanish, i.e, $\langle(h'_{ij}(x_j,\tau)-\langle h'_{ij}(x_j,\tau)\rangle)\boldsymbol{r}_{ij}(x_j+d,\tau)\rangle\approx 0$, $\langle(h'_{ij}(x_j+d,\tau)-\langle h'_{ij}(x_j,\tau)\rangle)\boldsymbol{r}_{ij}(x_j,\tau)\rangle\approx 0$, $\langle\boldsymbol{r}_{ij}(x_j,\tau)\boldsymbol{r}_{ij}(x_j+d,\tau)\rangle\approx 0$, and therefore Eq. (14) is simplified to

$$\begin{aligned}&\langle(\dot{\boldsymbol{x}}_i(x_j,\tau)-\langle\dot{\boldsymbol{x}}_i(x_j,\tau)\rangle)(\dot{\boldsymbol{x}}_i(x_j+d,\tau)-\langle\dot{\boldsymbol{x}}_i(x_j,\tau)\rangle)\rangle\\&=\langle(h'_{ij}(x_j,\tau)-\langle h'_{ij}(x_j,\tau)\rangle)(h'_{ij}(x_j+d,\tau)-\langle h'_{ij}(x_j,\tau)\rangle)\rangle.\end{aligned}\tag{15}$$

Furthermore we define

$$\widetilde{h}_{ij}(x_j,\tau)=h'_{ij}(x_j,\tau)-\langle h'_{ij}(x_j,\tau)\rangle.\tag{16}$$

Based on Eqs. (13) and (16), when $d\to 0$, Eq. (15) is approximately written as

$$\mathrm{NNC}_{ij}(\tau)\approx\langle\widetilde{h}^2_{ij}(x_j,\tau)\rangle.\tag{17}$$

Now we analyze Eq. (17). When $\tau<\tau_{ij}$, the reset variable x_j has no direct effect on response variable x_i, thus $h'_{ij}(x_j,\tau)=0$ and $\widetilde{h}_{ij}(x_j,\tau)=0$, and furthermore $\mathrm{NNC}_{ij}(\tau)=0$. When $\tau=\tau_{ij}$, as the variable x_j has a direct effect on the variable x_i, significantly, $\mathrm{NNC}_{ij}(\tau)>0$. From $\tau<\tau_{ij}$ to $\tau=\tau_{ij}$, there exists a discontinuous increment, which depends on the interaction between node j and node i. Therefore, through calculating the nearest neighbor correlation with the time delay $\mathrm{NNC}_{ij}(\tau)$ via Eq. (13), we can infer the time delay τ_{ij} of node j to node i.

For measurable data Eq. (4), since sampling is discrete, $\mathrm{NNC}_{ij}(\tau)$ is equivalent to $\mathrm{NNC}_{ij}(n)$, where $\tau=n\Delta t$, $n=0,1,2,\ldots,n_{\max}$ denote the discrete delays. The discrete delay of an actual time delay τ_{ij} can be expressed by

$$n_{ij}=\left\lfloor\frac{\tau_{ij}}{\Delta t}\right\rfloor,\tag{18}$$

where $\lfloor\cdot\rfloor$ denotes integer output, and n_{ij} represents the discrete delay of node j to node i.

After the time delay τ_{ij} is determined, we rewrite Eq. (5) as

$$\dot{x}_i(t_m+\tau_{ij})=h'_{ij}(x_j(t_m),\tau_{ij})+b_{ij}(\tau_{ij})+r_{ij}(t_m+\tau_{ij}).\tag{19}$$

To solve Eq. (19), we assume that $h'_{ij}(x_j(t_m),\tau_{ij})+b_{ij}(\tau_{ij})$ can be expanded by a basis set $\boldsymbol{L}(x_j(t_m))=[1,L_1(x_j(t_m)),L_2(x_j(t_m)),\ldots,L_K(x_j(t_m))]^{\mathrm{T}}$,[38] where T denotes the transpose of a matrix. We further rewrite Eq. (19) as

$$\dot{x}_i(t_m+\tau_{ij})=\boldsymbol{A}_{ij}\cdot\boldsymbol{L}(x_j(t_m))+r_{ij}(t_m+\tau_{ij}),\tag{20}$$

where $\boldsymbol{A}_{ij}=[A_{ij,0},A_{ij,1},A_{ij,2},\ldots,A_{ij,K}]$, $A_{ij,0}=b_{ij}(\tau_{ij})$. $\boldsymbol{A}_{ij}$ can be solved by

$$\hat{\boldsymbol{A}}_{ij}=\langle x_i(t_m+\tau_{ij})\boldsymbol{L}^{\mathrm{T}}(x_j(t_m))\rangle\cdot\langle\boldsymbol{L}(x_j(t_m))\cdot\boldsymbol{L}^{\mathrm{T}}(x_j(t_m))\rangle^{-1},\tag{21}$$

where symbol $\hat{}$ represents the numerical result, and $^{-1}$ denotes the inverse of a matrix. $\langle\dot{x}_i(t_m+\tau_{ij})\boldsymbol{L}^{\mathrm{T}}(x_j(t_m))\rangle$ and $\langle\boldsymbol{L}(x_j(t_m))\cdot\boldsymbol{L}^{\mathrm{T}}(x_j(t_m))\rangle$ can be computed from data ensembles Eq. (4).

The reconstruction method can infer the time delay and equivalent coupling functions of node j to node i from measured data by arbitrarily resetting the variable of node j. Through calculating the nearest neighbor correlation $\mathrm{NNC}_{ij}(\tau)$ defined in Eq. (13), while τ ranges from 0 to the actual time delay τ_{ij}, we can find that $\mathrm{NNC}_{ij}(\tau)$ has a discontinuous increment, which can be used to find out the accurate time delay τ_{ij} of node j to node i. After the time delay τ_{ij} is determined, the equivalent directed time-delayed coupling function $h'_{ij}(x_j(t_m),\tau_{ij})$ can be further solved through Eq. (21). This method can detect all the equivalent time-delayed coupling functions of an entire network by arbitrarily resetting the variables of all nodes in the network.

3. Simulation results

3.1. Time-delayed coupled Lorenz networks

First, consider a time-delayed coupled Lorenz network[39]

$$\begin{aligned}\dot{x}_i(t)&=\sigma(y_i(t)-x_i(t))+\sum_{j\neq i}^{N}h_{ij}(x_j(t-\tau_{ij}),x_i(t))+\eta_i(t),\\\dot{y}_i(t)&=-x_i(t)z_i(t)+\mu x_i(t)-y_i(t),\\\dot{z}_i(t)&=x_i(t)y_i(t)-\beta z_i(t),\end{aligned}\tag{22}$$

where a linear diffusion coupling function of node j to node i, $h_{ij}(x_i(t),x_j(t-\tau_{ij}))=W_{ij}(x_j(t-\tau_{ij})-x_i(t))$, is chosen. W_{ij} is the coupling coefficient of node j to node i. W_{ij} is uniformly distributed in $[0.2,1.0]$ and $[-1.0,-0.2]$. The time delays τ_{ij}

are uniformly distributed in $[0,0.5]$. A random network with the connection probability $p=0.15$ is chosen and the network size is $N=40$. The local dynamic parameters $\sigma=10$, $\mu=30$, and $\beta=8/3$, and thus the dynamics of the network are chaotic. η_i denotes white noises as in Eq. (3). In the following simulations, if the noise intensity is not specified, the default is $Q_i=10$.

We assume that variable x_i is measurable and variables y_i and z_i are unmeasurable. We randomly reset variable x_1 distributed uniformly within $[-20,20]$ and acquire the data Eq. (4). Resetting time intervals τ_{reset} are uniformly distributed in $[1,2]$. Our task is to use these data to infer the time delays τ_{i1} and coupling coefficients W_{i1}. Selecting $i=5$, $\tau_{51}=0.308$ is the time delay of node 1 to node 5, and $W_{51}=0.944$ is the coupling coefficient of node 1 to node 5. Given a sampling interval $\Delta t=0.006$, then $\tau_{51}=51.33\Delta t$, and thus the discrete delay $n_{51}=51$. Choosing $\tau=n\Delta t$, we calculate $\dot{x}_i(t_m+\tau)$ from measured data by the forward difference $\dot{x}_i(t_m+\tau)=[x_i(t_m+\tau+\Delta t)-x_i(t_m+\tau)]/\Delta t$. Then we smooth these results via Eq. (9) with $M=5\times10^5$ and $d=0.4$. The smoothing curves of $\dot{x}_5(x_1,\tau)$ when $\tau=0,0.300(50\Delta t),0.306(51\Delta t),0.312(52\Delta t)$ are plotted in Figs. 1(a)–1(d). In Fig. 1(a) ($\tau=0$) and Fig. 1(b) ($\tau=50\Delta t$), the smoothed data display randomness, i.e., no dependence. In fact, when τ ranges from 0 to $50\Delta t$, node 5 has not been affected by node 1 due to the time delay; $\dot{x}_5(x_1,\tau)$ maintains such randomness. When $\tau=51\Delta t$ (Fig. 1(c)) and $52\Delta t$ (Fig. 1(d)), the smoothed data display a linear dependence. In Fig. 1(c), the graph represents $\tau=51\Delta t$, you may observe the calculated $\dot{x}_5(x_1,\tau)$ has already been affected by the reset variable x_1. The reason for that is because we are using forward difference. Thus, the affection looks like happen before the real time delay $\tau_{51}=51.33\Delta t$.

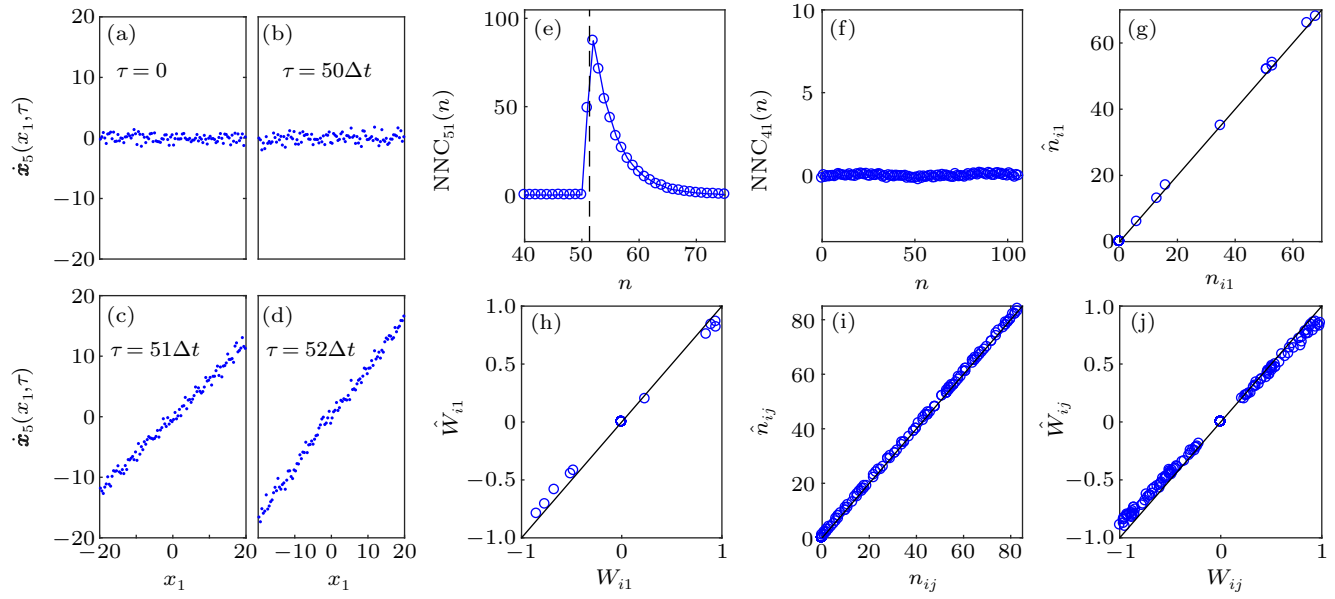


Fig. 1. Simulation results of Eq. (22) with linear diffusion coupling functions $h_{ij}(x_i(t),x_j(t-\tau_{ij}))=W_{ij}(x_j(t-\tau_{ij})-x_i(t))$. Data volume $M=5\times10^5$ and sampling interval $\Delta t=0.006$. The actual time delay of node 1 to node 5 $\tau_{51}=0.308$, $\tau_{51}=51.33\Delta t$, and the discrete time delay $n_{51}=51$. Left: Smoothing curves $\dot{x}_5(x_1,\tau)$ for (a) $\tau=0$, (b) $\tau=0.300$ $(50\Delta t)$, (c) $\tau=0.306$ $(51\Delta t)$, (d) $\tau=0.312$ $(52\Delta t)$ vs. the state variable x_1. The curves have no dependence on x_1 (a), (b) and a linear dependence (c), (d). Right: (e) Dependence of NNC_{51} on discrete time delay n. The dashed line marks the actual time delay $\tau_{51}/\Delta t=51.33$. (f) Dependence of NNC_{41} on n. (g) Reconstructed discrete delays $\hat{n}_{i1}$ plotted against the actual discrete delays n_{i1}. (h) Reconstructed coupling $\hat{W}_{i1}$ plotted against the actual W_{i1}. (i) Reconstructed $\hat{n}_{ij}$ plotted against the actual n_{ij}. (j) Reconstructed $\hat{W}_{ij}$ plotted against the actual W_{ij}.

We calculate $\mathrm{NNC}_{51}(n)$ via Eq. (13), where $n=\lfloor\tau/\Delta t\rfloor$, and the results (circles) are shown in Fig. 1(e). In Fig. 1(e), the dashed line marks the actual time delay $\tau_{51}/\Delta t=51.33$, which is located between the first non-zero point ($n=51$) and the second non-zero point ($n=52$). We can observe that $\mathrm{NNC}_{51}(50)=0$, and $\mathrm{NNC}_{51}(51)$ and $\mathrm{NNC}_{51}(52)$ have a significant increment. The increments originate from the effect of the delay and the forward difference calculation of $\dot{x}_5(t_m+\tau)$. Here we choose the larger of the two non-zero values, i.e., $\hat{n}_{51}=52$ as the reconstructed discrete delay. If $\tau_{ij}/\Delta t$ is not an integer, the maximal error of reconstructed time delay $\hat{\tau}_{ij}=\hat{n}_{ij}\Delta t$ is a sampling interval, where $\hat{n}_{ij}$ is the numerical discrete delay of node j to node i. For comparison, we select node 4 and calculate $\mathrm{NNC}_{41}(n)$, and the results are presented in Fig. 1(f). Due to no link of node 1 to node 4, the values of $\mathrm{NNC}_{41}(n)$ are near to zero and there is no significant increment point. Comparing Fig. 1(e) with Fig. 1(f), we conclude that we can determine time delays by random variable resetting via Eq. (13).

In Fig. 1(g), we plot the curve of numerical $\hat{n}_{i1}$ against the actual n_{i1}. The results show that the numerical $\hat{n}_{i1}$ values are consistent with the actual values. After determining the time delays, we can select suitable bases $\boldsymbol{L}=[1,x_1]^{\mathrm{T}}$ according to the linear dependence shown in Fig. 1(d), and then coefficients $A_{i1,1}$ of variable x_1 are used as estimates of the coupling coefficients $\hat{W}_{i1}$, which also show good agreement

with the actual coupling coefficients W_{i1} as in Fig. 1(h). Then we randomly selected 20 nodes in the network to reset, and the inferred time delays $\hat{n}_{ij}$ and coupling coefficients $\hat{W}_{ij}$ of these 20 nodes to all nodes are shown against the actual values n_{ij} and W_{ij} in Figs. 1(i) and 1(j). We can observe that the numerical $\hat{n}_{ij}$ values are consistent with the actual values n_{ij}, but there is some deviation in the numerical coupling coefficients $\hat{W}_{ij}$. Because of discrete time sampling, the error of detected time delays depends on the sampling interval Δt. The error of detected time delays can cause deviations of interactions and the deviations further make reconstructed coupling coefficients decrease or increase. Therefore, the deviations of determined coupling coefficients depend on specific coupling functions, state variables, and the error of time delays.

We will discuss how the number of resets M and the sampling interval Δt affect the reconstruction results. We use the root-mean-square errors E_τ and E_W to evaluate the reconstruction results $\hat{\tau}_{ij}$ and $\hat{W}_{ij}$,

$$E_\tau = \sqrt{\frac{\sum_{i=1}^{N}\sum_{j=1,j\neq i}^{N}(\hat{\tau}_{ij}-\tau_{ij})^2}{N\times(N-1)}},$$

$$E_W = \sqrt{\frac{\sum_{i=1}^{N}\sum_{j=1,j\neq i}^{N}(\hat{W}_{ij}-W_{ij})^2}{N\times(N-1)}}.$$

Figure 2 represents the errors of the calculated time delays E_τ (Fig. 2(a)) and the calculated coupling coefficients E_W (Fig. 2(b)). In Fig. 2(a), due to the influence of fluctuations r_{ij}, the errors of time delays E_τ are greater for a relatively small number of resets M. As M increases, the reconstruction error E_τ reduces until it reaches saturation, which depends on sampling interval Δt. This is because when the amount of data is large enough, the errors of time delays are determined by sampling interval Δt and the maximum deviation of a time delay is less than Δt. In Fig. 2(b), we can observe that, as the amount of data increases, the errors of the coupling coefficient decrease until a saturation state is reached. The errors of coupling coefficients mainly originate from sampling interval Δt, thus, to reduce the errors of coupling coefficients, decreasing sampling interval Δt is more effective than increasing the amount of data M.

In Eq. (22), nonlinear interactions, $h_{ij}(x_i(t),x_j(t-\tau_{ij})) = W_{ij}x_j^2(t-\tau_{ij})$, are considered and the numerical results are represented in Fig. 3. To avoid system divergence, we decrease the coupling coefficients W_{ij} and they are reduced to one tenth of the original values. We plot the curve of $\dot{x}_5(x_1,\tau)$ against x_1 shown in Fig. 3(a), while $\tau = 52\Delta t$. $\mathrm{NNC}_{51}(n)$ are calculated by using Eq. (13) and the results are shown in Fig. 3(b). Figure 3(b) is similar to Fig. 1(e), and we can observe that the actual time delay $\tau_{51}/\Delta t = 51.33$ is smaller than the second non-zero point and greater than the first non-zero point. We select the second non-zero point as the numerical discrete delay, i.e., $\hat{n}_{51} = 52$. Similarly, after determining the time delay τ_{ij}, we select basis $\boldsymbol{L} = [1, x_j^2]^{\mathrm{T}}$ and solve the coupling coefficient $\hat{W}_{ij}$. The curves of Figs. 3(c) and 3(d) are similar to those of Figs. 1(i) and 1(j).

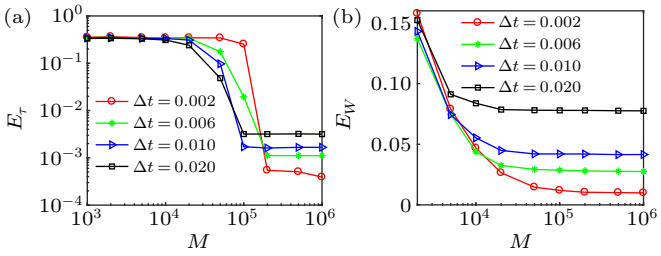


Fig. 2. The root-mean-square error E_τ of reconstruction time delays and the root-mean-square error E_W of coupling coefficients are shown in (a) and (b), respectively. (a) Dependence of E_τ on M for $\Delta t = 0.002, 0.006, 0.010$, and 0.020. (b) Dependence of E_W on M.

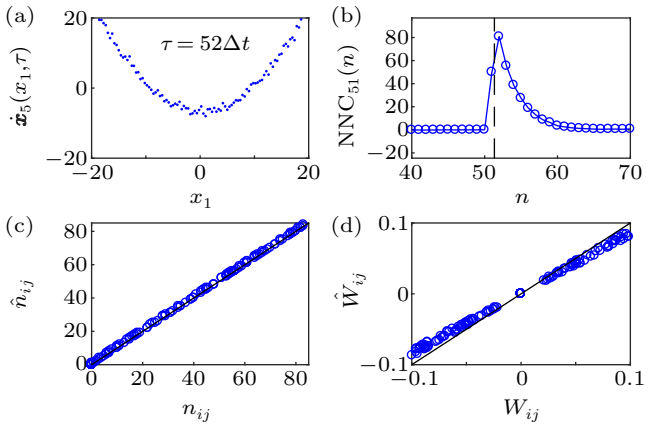


Fig. 3. Simulation results of Eq. (22) with nonlinear coupling functions $h_{ij}(x_j(t-\tau_{ij}),x_i(t)) = W_{ij}x_j^2(t-\tau_{ij})$. $M = 5\times10^5$ and $\Delta t = 0.006$, $\tau_{51} = 0.308$. (a) Smoothing curves of $\dot{x}_5(x_1,\tau)$ plotted against x_1 at $\tau = 0.312$ ($52\Delta t$). (b) Dependence of NNC_{51} on n. The dashed line marks the actual time delay $\tau_{51}/\Delta t = 51.33$. (c) Numerical $\hat{n}_{ij}$ plotted against the actual n_{ij}. (d) Numerical $\hat{W}_{ij}$ plotted against the actual W_{ij}.

3.2. Time-delayed Hodgkin–Huxley neural network

We consider time-delayed Hodgkin–Huxley[40] neural network dynamics,

$$\begin{aligned} C_{m,i}\dot{V}_i = & -g_{\mathrm{L},i}(V_i-E_\mathrm{L}) - g_{\mathrm{Na},i}m_i^3h_i(V_i-E_\mathrm{Na}) \\ & -g_{\mathrm{K},i}n_i^4(V_i-E_\mathrm{K}) + I_i^{(\mathrm{in})} + I_i^{(\mathrm{syn})}, \end{aligned} \tag{23}$$

where V_i is the membrane potential of the i-th neuron in the network, and V_i is measurable. All the parameters are uniformly distributed, $C_{m,i} \in [0.9, 1.1]$ μF/cm^2, $g_{\mathrm{L},i} \in [0.25, 0.35]$ ms/cm^2, $g_{\mathrm{Na},i} \in [110, 130]$ ms/cm^2, $g_{\mathrm{K},i} \in [30, 40]$ ms/cm^2, $E_\mathrm{L} \in [-11.1, -10.1]$ mV, $E_\mathrm{Na} \in [110, 130]$ mV, $E_\mathrm{K} \in [-30, -20]$ mV, and $I_i^{(\mathrm{in})} \in [6,\ 12]$ μA/cm^2. $I_i^{(\mathrm{syn})}$ is synapse current expressed by

$$I_i^{(\mathrm{syn})} = \sum_{j\neq i}^{N} W_{ij}\frac{V_\mathrm{rev}-V_i}{1+\exp(-(V_j(t-\tau_{ij})-V_\mathrm{th})/\sigma)}, \tag{24}$$

where the coupling coefficients W_{ij} are uniformly distributed in $[0.04, 0.2]$ and $[-0.2, -0.04]$ for excitatory and inhibitory synapses, respectively, and $W_{ij} = 0$ for no links. The ratio of excitatory synapses to inhibitory synapses is 4 : 1. The time

delays τ_{ij} are uniformly distributed in $[0,1.0]$. The structure of this network is exactly the same as that of Eq. (22). The parameters $V_{\rm rev}=110$ mV, $V_{\rm th}=100$ mV, and $\sigma=0.01$. Gate variables m_i, h_i, n_i are expressed by

$$\begin{aligned}\dot{m}_i &= \alpha_{m,i}(V_i)(1-m_i)-\beta_{m,i}(V_i)m_i,\\ \dot{h}_i &= \alpha_{h,i}(V_i)(1-h_i)-\beta_{h,i}(V_i)h_i,\\ \dot{n}_i &= \alpha_{n,i}(V_i)(1-n_i)-\beta_{n,i}(V_i)n_i,\end{aligned} \tag{25}$$

where $\alpha_{m,i}=(2.5-0.1V_i)/(\mathrm{e}^{2.5-0.1V_i}-1)$, $\beta_{m,i}=4\mathrm{e}^{-V_i/18}$, $\alpha_{h,i}=0.07\mathrm{e}^{-V_i/20}$, $\beta_{h,i}=1/(\mathrm{e}^{3-0.1V_i}+1)$, $\alpha_{n,i}=(0.1-0.01V_i)/(\mathrm{e}^{1-0.1V_i}-1)$, and $\beta_{n,i}=0.125\mathrm{e}^{-V_i/80}$. All gate variables m_i, h_i, n_i are unmeasurable.

Without loss of generality, we arbitrarily reinitialize the membrane potential of node 1, $V_1\in[-30,110]$ with $\tau_{\rm reset}\in[30,40]$. We set the sampling interval $\Delta t=0.008$ and the number of resets $M=10^5$. In Fig. 4(a), we plot the curves of the smoothed $\dot{\bar{V}}_5(V_1,\tau)$ with $\tau=0.616$ $(77\Delta t)$. The actual time delay of node 1 to node 5 $\tau_{51}=0.6161$ $(77.0125\Delta t)$. When and only when variable V_1 exceeds $V_{\rm th}=100$ mV, neuron 1 has a significant effect on the postsynaptic neuron 5. Similar to as in Fig. 3(b), we plot the curves of $\mathrm{NNC}_{51}(n)$. The dashed line marks the actual time delay $\tau_{51}/\Delta t=77.0125$, which is near to the first non-zero point ($\hat{n}_{51}=77$). By resetting every node, we infer all discrete delays $\hat{n}_{ij}$ and the results are shown in Fig. 4(c). We can see that the reconstructed time delays display satisfactory results. Selecting $[1,1/(1+\mathrm{e}^{-(V_j-V_{\rm th})/\sigma})]^{\rm T}$ as the basis, estimated coupling coefficients of $1/(1+\mathrm{e}^{-(V_j-V_{\rm th})/\sigma})$ are $\hat{W}'_{ij}=W_{ij}C_{m,i}\langle V_{\rm rev}-V_i\rangle$, with $\hat{W}_{ij}=\hat{W}'_{ij}/\left(C_{m,i}\langle V_{\rm rev}-V_i\rangle\right)$ as the estimates of actual W_{ij}. The results are represented in Fig. 4(d). Similar to as in Fig. 3(d), the numerical coefficients also have deviation.

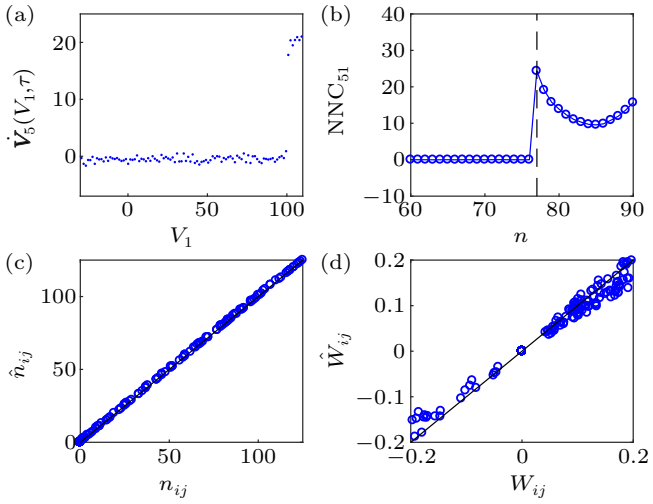


Fig. 4. Simulation results of a time-delayed Hodgkin–Huxley neural network. Set sampling interval $\Delta t=0.008$ and the reset number $M=10^5$. The actual time delay of node 1 to node 5 $\tau_{51}=0.6161$ $(77.0125\Delta t)$. (a) $\dot{\bar{V}}_5(V_1,\tau)$ plotted against V_1 at $\tau=0.616$ $(77\Delta t)$. (b) NNC_{51} plotted against n. The dashed line marks the actual time delay $\tau_{51}/\Delta t=77.0125$. (c) Numerical $\hat{n}_{ij}$ plotted against the actual n_{ij}. (d) Numerical $\hat{W}_{ij}$ plotted against the actual W_{ij}.

4. Discussion

We can detect the equivalent coupling functions of time-delayed dynamic networks by the random state variable resetting method. To determine the time delay τ_{ij} of node j to node i, we define the nearest neighbor correlation function $\mathrm{NNC}_{ij}(\tau)$, and calculate $\mathrm{NNC}_{ij}(\tau)$ from measurable data, where $\tau=n\Delta t$, $n=0,1,2,\ldots,n_{\max}$. Based on the increment of $\mathrm{NNC}_{ij}(\tau)$ at the actual time delay, we can well determine the time delay τ_{ij}. The error of the reconstructed time delay is less than a sampling interval. After the time delay is determined, the equivalent coupling function can further be reconstructed from measurable data. This method can acquire all the time delays and all the equivalent coupling functions of the entire network by arbitrarily resetting the state variables of all the nodes in the network. Because the reconstruction of any time-delayed interaction in the network can be achieved only with the data of two related nodes, this method is applicable to networks with hidden variables and nodes.

In Ref. [36], Zhang *et al.* proposed a method to detect time delays through fast-varying noises (FVN). Ideal fast-varying noises are white noises. Under the condition of discrete sampling, to infer the time delay τ_{ij} of node j to node i, we define a correlation function[36]

$$R_{ij}(n)=\langle\ddot{x}_i(t)x_j(t-n\Delta t)\rangle. \tag{26}$$

The increment of $R_{ij}(n)$ at n satisfies the following form:

$$\begin{aligned}\Delta_{ij}(n) &= R_{ij}(n-1)-R_{ij}(n)\\ &\approx \frac{1}{2}J_{ij}Q_j(\delta_{n_{ij},n}+\delta_{n_{ij}-1,n})+H_{ij}(n)\Delta t,\end{aligned} \tag{27}$$

where

$$J_{ij}=\left\langle\frac{\partial h_{ij}(x_i(t),x_j(t-\tau_{ij}))}{\partial x_j(t-\tau_{ij})}\right\rangle$$

represents the average coupling strength of node j to node i and Q_j is the intensity of the white noise injected to node j. In Eq. (27), the contribution of other factors can be simplified as the second term $H_{ij}(n)\Delta t$.

In Eq. (27), we can observe, if $\Delta t\to 0$, $R_{ij}(n)$ is discontinuous at $n=n_{ij}$ and $n=n_{ij}-1$. Based on this discontinuity, we can determine the time delay $\tau_{ij}=n_{ij}\Delta t$. Furthermore, J_{ij} can be estimated via $\hat{J}_{ij}=\left[\Delta_{ij}(n_{ij})+\Delta_{ij}(n_{ij}+1)\right]/Q_j$, where Q_j is calculated through $\hat{Q}_j=\langle\dot{x}_j(t)x_j(t+\Delta t)\rangle-\langle\dot{x}_j(t)x_j(t)\rangle$.

We utilize the FVN method to analyze Eq. (22) with a linearly coupled Lorenz network. The results are illustrated in Figs. 5(a)–5(c), where the actual time delay $\tau_{51}=0.308$. We calculate $R_{51}(n)$ for $\Delta t=0.002$ (Fig. 5(a)), $\Delta t=0.010$ (Fig. 5(b)) and $\Delta t=0.020$ (Fig. 5(c)). We can observe that in Fig. 5(a), there exist significant increments at $n=153$ and $n=154$. However, as we increase Δt to 0.010 and 0.020, this method fails. The reconstructed results using our method are represented in Figs. 5(d) ($\Delta t=0.002$), 5(e) ($\Delta t=0.010$), and

5(f) ($\Delta t = 0.020$). It can be seen that our method can accurately identify the time delay even when the sampling interval is relatively large.

For linear diffusive coupling function $h_{ij}(x_i(t), x_j(t-\tau_{ij})) = W_{ij}(x_j(t-\tau_{ij}) - x_i(t))$, average coupling strength

$$J_{ij} = \left\langle \frac{\partial h_{ij}(x_i(t), x_j(t-\tau_{ij}))}{\partial x_j(t-\tau_{ij})} \right\rangle = W_{ij}.$$

We further calculate the time delays and coupling strengths by using the FVN method and our method (RSVR). The numerical discrete delays $\hat{n}_{i1}$ and coupling strengths $\hat{W}_{i1}$ for sampling interval $\Delta t = 0.002$ are illustrated in Figs. 6(a) and 6(b). We can see the numerical time delays for the two reconstruction methods display satisfactory results and the numerical coupling strengths have some deviations. Comparing with Fig. 1(j) ($\Delta t = 0.006$), since sampling interval $\Delta t = 0.002$ has decreased, the deviations clearly decrease.

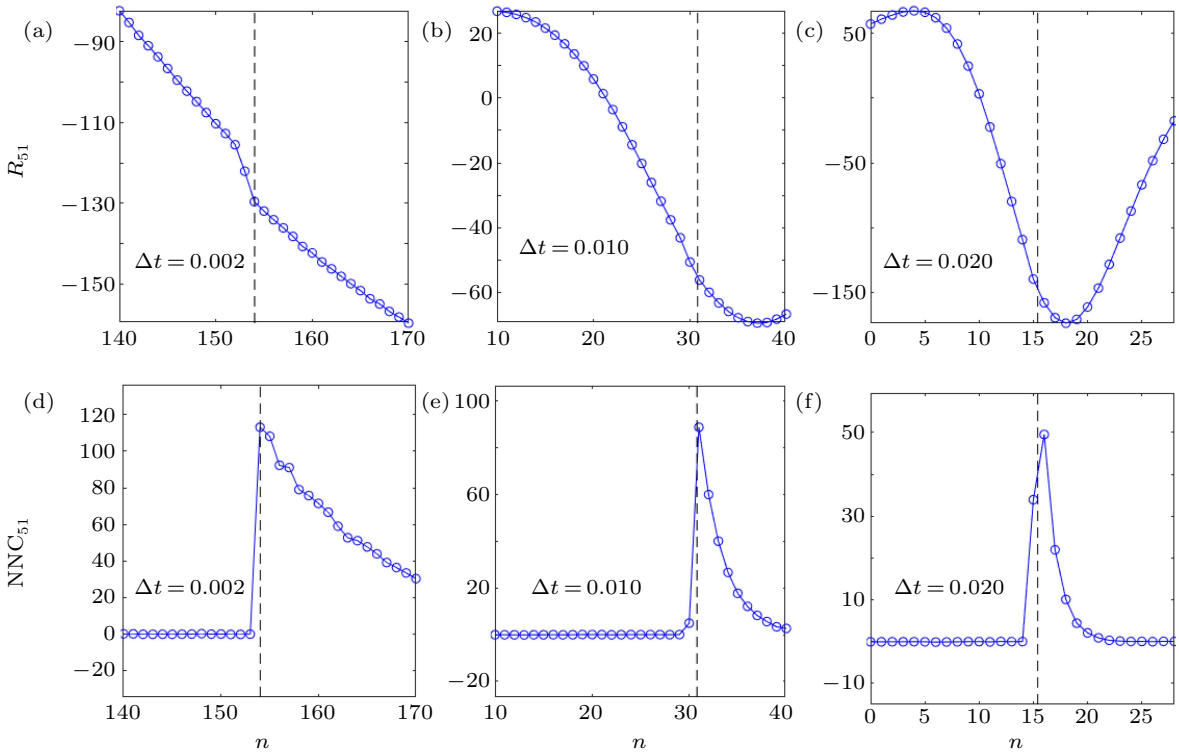


Fig. 5. Comparison of our method and the FVN method[36] for the example of a linearly coupled Lorenz network as in Eq. (22). All the dashed lines represent the actual time delay n_{ij}, $\tau_{ij} = n_{ij}\Delta t$. (a) $\Delta t = 0.002$ and the amount of data $N_{\mathrm{data}} = 10^9$. (b) $\Delta t = 0.010$ and $N_{\mathrm{data}} = 2 \times 10^8$. (c) $\Delta t = 0.010$ and $N_{\mathrm{data}} = 10^8$. (d) $\Delta t = 0.002$. (e) $\Delta t = 0.010$. (f) $\Delta t = 0.020$. The number of resets $M = 5 \times 10^4$ in (d)–(f).

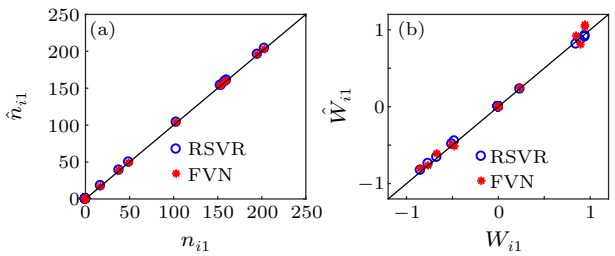


Fig. 6. The numerical discrete delays $\hat{n}_{i1}$ and coupling coefficients $\hat{W}_{i1}$ for the FVN method and our method (RSVR). $\Delta t = 0.002$. (a) The numerical $\hat{n}_{i1}$ plotted against the actual n_{i1}. (b) The numerical $\hat{W}_{i1}$ plotted against the actual W_{i1}.

Both our method and the FVN[36] method can reconstruct time-delayed interactions of dynamic networks with noises, hidden variables and nodes. For these two methods, detection of the interaction between two nodes only needs the output of these two nodes, so network sizes and structures do not affect the calculated results significantly. Only average coupling strength can be inferred through the FVN method,[36] while our method can reconstruct the equivalent coupling function no matter whether it is linear as in Fig. 1(d) or nonlinear as in Figs. 3(a) and 4(a). Moreover, our method has better robustness for sampling intervals.

Finally, we consider weak couplings. For a very weak coupling, if $W_{ij} \to 0$, the equivalent coupling function $h'_{ij}(x_j, \tau_{ij}) \to 0$ and $\widetilde{h}_{ij}(x_j, \tau) \to 0$ (Eq. (16)). According to Eq. (17), $\mathrm{NNC}_{ij}(\tau_{ij}) \to 0$, and we cannot observe a significant increment for $\mathrm{NNC}_{ij}(\tau_{ij})$. Thus we cannot identify actual time delay τ_{ij}, and then W_{ij} is also not available.

5. Conclusion

In this paper, we introduced a random state variable resetting method to detect the coupling functions of time-delayed dynamic networks. The nearest neighbor correlation function has been defined and calculated for measurable data by arbitrarily resetting the variable of j. The time delay of node j to node i can be determined by utilizing the increment of the nearest neighbor correlation at the actual time delay. The error of a reconstructed time delay only depends on the sampling

interval. Our proposed method has satisfactory reconstruction results for time delays even if the sampling interval is relatively large. Based on the determined time delays, the equivalent coupling functions can be estimated. Simulation results demonstrated that the random state variable resetting method and the nearest neighbor correlation function proposed can be used to detect the interactions of time-delayed dynamic networks.

References

[1] Newman M E J 2003 *SIAM Review* **23** 094206
[2] Boccaletti S, Latora V, Moreno Y, Chavez M and Hwang D U 2006 *Phys. Rep.* **424** 175308
[3] Timme M and Casadiego J 2014 *J. Phys. A: Math. Theor.* **47** 343001
[4] Zhang L S, Gu W F, Hu G and Mi Y Y 2014 *Chin. Phys. B* **23** 108902
[5] Sun J C 2016 *Chin. Phys. Lett.* **33** 100503
[6] Zhang M, Wang X J, Jin L and Liao Z H 2020 *Chin. Phys. B* **29** 096401
[7] Han F, Wang Z J and Fan H 2015 *Chin. Phys. Lett.* **32** 040502
[8] Rihan F A, Alsakaji H J and Rajivganthi C 2020 *Adv. Differ. Equ.* 502
[9] Qian Y, Gao H, Yao C, Cui X and Ma J 2018 *Chin. Phys. B* **27** 108902
[10] Cao B, Gu H and Li Y 2021 *Chin. Phys. B* **11** 050502
[11] Fan Y, Wang Z, Xia J and Shen H 2021 *Chin. Phys. B* **30** 030202
[12] Garofalo M, Nieus T Massobrio P and Martinoia S 2009 *Plos One* e6482
[13] Zhou D, Xiao Y, Zhang Y, Xu Z and Cai D 2013 *Phys. Rev. Lett.* **111** 054102
[14] Bianco-Martinez E, Rubido N, Antonopoulos C G and Baptista M S 2016 *Chaos* **26** 043102
[15] Vicente R, Wibral M, Lindner M and Pipa G 2011 *J. Comput. Neurosci.* **30** 45-67
[16] Zhang Z, Zheng Z, Niu H, Mi Y, Wu S and Hu G 2014 *Phys. Rev. E* **91** 012814
[17] Ching Emily S C, Lai P Y and Leung C Y 2015 *Phys. Rev. E* **91** 030801
[18] Chen Y, Zhang Z, Wang S and Hu G 2017 *Sci. Rep.* **7** 44639
[19] Casadiego J and Timme M 2018 *New J. Phys.* **20** 113031
[20] Wang W X, Lai Y C and Grebogi C 2016 *Phys. Rep.* 644
[21] Casadiego J, Nitzan M, Hallerberg S and Timme M 2017 *Nat. Commun.* **8** 2192
[22] Chen Y, Zhang Z, Chen T, Wang S and Hu G 2017 *Sci. Rep.* **7** 44639
[23] Zhang H F and Wang W X 2020 *Acta Phy. Sin.* **69** 088906 (in Chinese)
[24] Zhang Z Y, Chen Y, Mi Y Y and Hu G 2020 *Acta Phy. Sin.* **50** 010502 (in Chinese)
[25] Shi R, Hu G and Wang S 2019 *Commun. Nonlinear Sci. Numer. Simul.* **72** 407-416
[26] Jiang W, Wang Z and Wang S 2021 *Eur. Phys. J. B* **94** 138
[27] Zhang C, Chen Y and Hu G 2017 *Phys. Lett. A* **381** 2502
[28] Shi R, Jiang W and Wang S 2020 *Chaos* **30** 013138
[29] Levnajić Z and Pikovsky A 2011 *Phys. Rev. Lett.* **107** 034101
[30] Bezruchko B P, Karavaev A S, Ponomarenko V I and Prokhorov M D 2001 *Phys. Rev. E* **64** 056216
[31] Cimponeriu L, Rosenblum M and Pikovsky A 2004 *Phys. Rev. E* **70** 046213
[32] Siefert M 2007 *Phys. Rev. E* **76** 026215
[33] Ponomarenko V I and Prokhorov M D 2009 *Phys. Rev. E* **80** 066206
[34] Zunino L, Soriano M C, Fischer I, Rosso O A and Mirasso C R 2010 *Phys. Rev. E* **82** 046212
[35] Ma H, Leng S, Tao C, Ying X, Kurths J and Lai Y C 2017 *Phys. Rev. E* **96** 012221
[36] Zhang Z, Chen Y, Mi Y and Hu G 2019 *Phys. Rev. E* **99** 042311
[37] Shi R, Deng C and Wang S 2018 *Europhys. Lett.* **124** 18002
[38] Deng C, Jiang W and Wang S 2021 *Chaos* **31** 033146
[39] Lorenz E N 1963 *J. Atmos. Sci.* **20** 130
[40] Hodgkin A L and Huxley A F 1952 *J. Physiol.* **117** 500-544